



Assessment of heat storage integration for water vapour compression heat pumps: thermodynamic and techno-economic perspectives

Seon Tae Kim, Steffen Klöppel, Eberhard Nicke, K. Malleswararao, Marc Linder & Panagiotis Stathopoulos

To cite this article: Seon Tae Kim, Steffen Klöppel, Eberhard Nicke, K. Malleswararao, Marc Linder & Panagiotis Stathopoulos (2025) Assessment of heat storage integration for water vapour compression heat pumps: thermodynamic and techno-economic perspectives, *International Journal of Sustainable Energy*, 44:1, 2433580, DOI: [10.1080/14786451.2024.2433580](https://doi.org/10.1080/14786451.2024.2433580)

To link to this article: <https://doi.org/10.1080/14786451.2024.2433580>



© 2024 The Author(s). Published by Informa UK Limited, trading as Taylor & Francis Group



Published online: 05 Dec 2024.



Submit your article to this journal [↗](#)





View related articles [↗](#)



View Crossmark data [↗](#)

Assessment of heat storage integration for water vapour compression heat pumps: thermodynamic and techno-economic perspectives

Seon Tae Kim ^a, Steffen Klöppel ^a, Eberhard Nicke^a, K. Malleswararao ^b,
Marc Linder ^b and Panagiotis Stathopoulos^a

^aInstitute of Low-Carbon Industrial Processes, German Aerospace Center (DLR), Cottbus/Zittau, Germany; ^bInstitute of Engineering Thermodynamics, German Aerospace Center (DLR), Stuttgart, Germany

ABSTRACT

The integrated system, consisting of a two-stage high-temperature heat pump (HTHP) and thermal energy storage (TES), has been proposed as an effective solution to reduce CO₂ emissions in industrial processes effectively.

The water vapour HTHP, which can supply heat at 200°C, demonstrated a coefficient of performance (COP) between 4.4 and 7.5. Two different TES systems were introduced: concrete sensible heat storage (SHS) and strontium bromide/water (SrBr₂/H₂O) thermochemical energy storage (TCES). While the concrete SHS is limited to temperature below 200°C, the SrBr₂/H₂O TCES can deliver heat between 196°C and 228°C with higher cycle efficiency. The integrated system of HTHP and SrBr₂/H₂O TCES achieved a net present value (NPV) of €464,559 and €182,374 over a 20-years lifespan, with internal rates of return (IRR) ranging from 15.8% to 23.6%.

This HTHP and TCES system has sufficient potential to replace fossil-fuel industrial boilers, leading to significant reduction in CO₂ emissions in industrial processes.

ARTICLE HISTORY

Received 26 October 2024

Accepted 19 November 2024

KEYWORDS

High-temperature heat pump; thermochemical energy storage; R-718 (water); multistage vapor compression cycle; thermodynamic analysis; techno economic analysis

1. Introduction

Global greenhouse gas (GHG) emissions have continued to increase over the last decades. Atmospheric carbon dioxide (CO₂) concentrations reached 410 parts per million (ppm), methane (CH₄) reached 1,866 parts per billion (ppb), and nitrous oxide (N₂O) researched 332 ppb in 2019. Since 1750, CO₂, CH₄, and N₂O are increased by 47%, 156%, and 23%, respectively. These values far exceed the multi-millennial changes between glacial and interglacial periods over the past 800,000 years (Lee et al. 2023).

Specifically, CO₂ emissions, which are a major contributor to global warming were estimated at approximately 36.8 Gt in 2022, showing a growth of 0.9%, 321 Mt. The industrial sector is responsible for approximately 35% of global GHG emissions when reallocated to the final energy consumption sectors (Edenhofer 2014; Lamb et al. 2021). Global industrial energy demand, which directly influences GHG emissions, has been steadily increasing, reaching approximately 165 EJ in 2021, a 4% increase from 2019. Currently this sector accounts for more than 40% of global electricity demand (IEA 2023a; 2023b). In conclusion, industrial energy demand accounted for

CONTACT Seon Tae Kim  seon.kim@dlr.de

approximately 38% of the total final energy demand in 2022, up from 33% in 2000, with fossil fuels representing more than half of total final energy demand in the industrial sector (IEA 2021; 2022a).

Among the various energy services in the industry, heating applications offer the largest potential for electrification. Thermal energy demand is dominant in the industrial sector, with each sub-sector having its specific temperature requirements (IEA 2021). Waste heat recovery and upgrade with heat pumps presents an excellent potential for enhancing the efficiency of existing industrial processes (Brueckner et al. 2014; Huang et al. 2017).

Electrifying high-temperature heat ($>400^{\circ}\text{C}$) in industry poses great challenges. Nevertheless, many electrification technologies are already commercially available or under development for low ($<100^{\circ}\text{C}$) and medium ($100\text{--}400^{\circ}\text{C}$) temperature heat applications (IEA 2023b). In particular, heat pumps offer significant potential across various sectors and can play an important role in decarbonising industrial heat supply at temperatures below 200°C . This temperature range is primarily required in sectors such as pulp and paper, food and beverage, and the chemical industry (Tobias et al. 2016). Globally industrial process heat within the $100\text{--}200^{\circ}\text{C}$ range accounts for approximately 20% (22.1 EJ) of total industrial energy consumption (IEA 2022b; Rehfeldt, Fleiter, and Toro 2018). Within the EU 28, specifically in the paper and food sub-sectors, industrial heat pumps can cover around 69% and 51% of the heat demand, respectively (Marina et al. 2021).

Nonetheless, with the increasing adoption of industrial HTHP and the utilisation rate of renewable energy, an accompanying rise in the imbalance between supply and demand is anticipated, necessitating the development of energy storage systems to mitigate this challenge and enhance grid flexibility (Tong et al. 2021). Among the various energy storage technologies, thermal energy storage (TES) has a higher energy density and longer storage duration than other storage methods (Kim, Takasu, and Kato 2021). Moreover, TES offers a more cost-effective solution for longer-term storage, and it can be designed to operate at high temperatures, such as for steam generation, industrial heating, thermal desalination (Augustine and Blair 2021; Kim, Takasu, and Kato 2023; Laing et al. 2011). Thermal energy storage systems are designed to store heat or cold for later use at different temperatures and locations, primarily to address the mismatch between energy generation and demand (Miró, Gasia, and Cabeza 2016). There are three primary types of TES systems: sensible heat storage, latent heat storage, and thermochemical heat storage. Sensible heat storage (SHS) involves storing heat by changing the temperature of the storage material. Latent heat storage relies on the phase transition of materials, typically a solid–liquid phase change, which allows for the storage of large amounts of heat at a constant temperature during the phase transition. Thermochemical energy storage (TCES) uses the heat generated through chemical reactions with high energy content, effectively storing energy. TES technology, particularly TCES, is considered an efficient system that can enhance the performance of heat pumps by delivering heat directly to industrial processes at high temperature. Additionally, it has the potential to expand the utilisation of low-cost variable renewable electricity in the industrial sector, bypassing the grid (IEA 2023b; Osterman and Stritih 2021).

The current study concentrates on comparing the integration of a SHS and TCES with a high-temperature heat pump (HTHP) cycle capable of delivering heat at 200°C . The system configuration and operating parameters are informed and further refined based on insights from the preliminary study (Kim et al. 2023a). The HTHP system is a two-stage water vapour (R-718) Rankine cycle with intercooling, which has been demonstrated to provide process heat within the temperature range of 100°C to 200°C (Kim et al. 2023b). Detailed operational strategies for the HTHP and TES systems are presented, with particular emphasis on enhancements to the operational logic of the SHS system, as informed by previous analyses. Through a comprehensive assessment of thermodynamic performance and techno-economic characteristics of integrated systems under HTHP operating conditions, this study identifies the inherent limitations of conventional SHS systems and evaluates the potential of TCES systems to complement and enhance the functionality of HTHP systems.

2. Modelling of thermodynamic and economic systems

2.1. Multistage water vapour compression cycle

A two-stage water vapour compression cycle with intercooling was introduced as the HTHP cycle, as shown in Figure 1. First water vapour is compressed to an intermediate pressure and then cooled close to its condensation temperature. The resulting slightly superheated steam is recompressed to the final pressure, corresponding to the aimed HTHP delivery temperature. The International Association for the Properties of Water and Steam (IAPWS-IF97), was adopted to calculate the water/steam properties in the HTHP cycle (International Association for the Properties of Water and Steam 2007).

The number of temperature conditions was significantly expanded from the preliminary study to facilitate a detailed investigation of the performance of the HTHP system alone, as well as the integrated system with the TES (Kim et al. 2023a). The temperature of the heat source, T_{source} , corresponding to waste heat, was fixed at 120°C. Consequently, the evaporation temperature, T_{evap} , was set at 90 and 100°C. The condensation temperature, T_{cond} , which is directly related to the discharge temperature, T_{dis} , was set to 130, 140, 150, and 160°C by considering the temperature lift limitation, which is up to 60–65 K when the pressure ratio is lower than 2.5 for each stage. As a result, the temperature difference, ΔT_{lift} , ranged from 30 to 70 K. The intermediate pressure was determined to maintain the same pressure ratio between the first and second stages, as previous work demonstrated that the two-stage cycle achieved the highest coefficient of performance (COP) when both compressors operated at the same pressure ratio (Kim et al. 2023b). Additionally, it was assumed that the temperature differences between the hot and cold sides after the heat exchangers were 10 K ($T_{\text{sup}} \& \text{sub}} = 10 \text{ K}$).

The heat sink flow, which passes through the intercooler and condenser, was set to supply a constant thermal power of 500 kW at 200°C to the TES system and was also used to retrieve heat from the TES system. The heat sink pressure was equal to the pressure at the condenser, $P_{\text{sink}} = P_{\text{cond}}$, and the mass flow rate of the heat sink remained constant during both the heat storage and release operation, $m_{\text{stor}} = m_{\text{rel}}$, of the TES system.

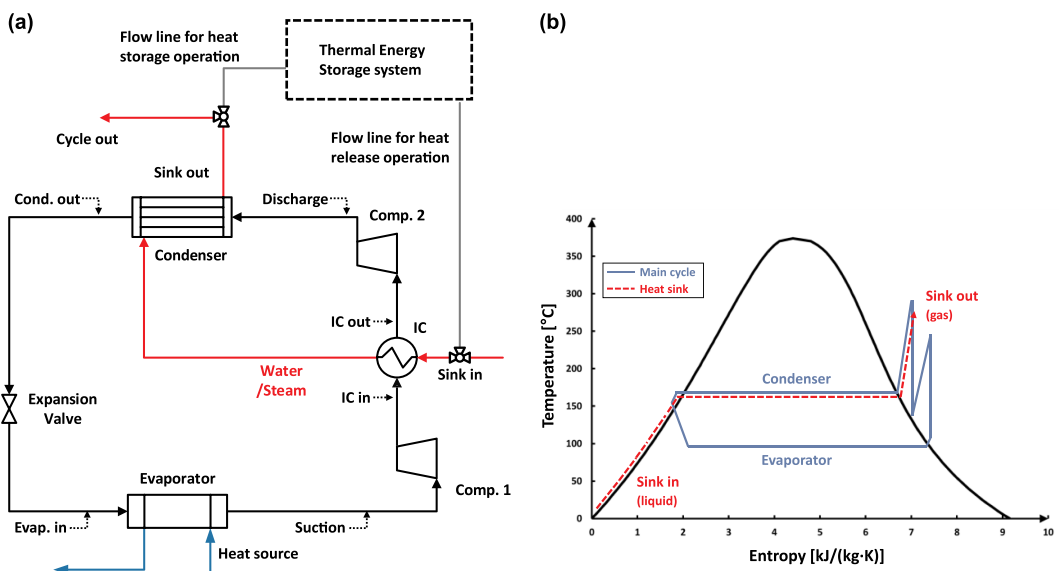


Figure 1. Image of (a) schematic diagram of the HTHP with TES system and (b) T-S diagram of HTHP cycle (Kim et al. 2023a).

2.2. Thermal energy storage systems

Sensible heat storage involves the use of a material to store thermal energy by virtue of increasing or decreasing the temperature of a storage medium. This energy storage method is widely used and is the most common type of TES technology. Many materials can be used for SHS materials, such as water, air, oil, rock beds, brick, concrete, and so on. In this study, an SHS system that using concrete is considered. Concrete can withstand cyclic stress at temperatures of up to 500°C during numerous consecutive charging and discharging periods, therefore, concrete is considered as suitable sensible heat storage material over long lifetimes (Laing et al. 2009).

The concrete SHS system in current study consists of two tanks: a hot tank containing concrete and a cold tank that stores air as a heat transfer fluid (HTF). The operational strategies are as follows. During the storage operation, low-temperature air, $T_{\text{amb}} = 25^\circ\text{C}$, in the cold tank is heated using high-temperature steam from the HTHP cycle and an electric heater, $T_{\text{stor}} = 200^\circ\text{C}$, for 8 hours, Figure 2(a). To specifically address the pinch point violation in the heat exchanger, which was overlooked in preliminary study, an electric heater has been introduced particularly. Due to the higher heat capacity, c , of water/steam compare to air, as well as the presence of phase change region, the air temperature of heat exchanger outlet is limited to 10 K above the condensation temperature. This constraint prevents pinch point violations in the heat exchanger, Figure 2(b). Subsequently, the electric heater, with an efficiency of 0.95, further elevates the air temperature to 200°C.

In the heat release operation, high-temperature air transfers heat to low-temperature water/steam in the heat sink, delivering thermal energy to meet demand, Figure 3. During the heat release operation, the cycle out temperature, $T_{\text{cycle out}}$ of SHS system can be controlled by regulating the mass flow rate of air from the hot tank to cold tank, Figure 3(a). Due to the differing properties of the two heat transfer fluids, a pinch point violation problem can also occur during the heat release operation. Therefore, the cycle out temperature, $T_{\text{cycle out}}$ has been restricted to not lower than 10 K below the condensation temperature, Figure 3(b). Furthermore, the heat release operation is limited to 16 hours, assuming that one cycle of TES operation is completed per day. As mentioned in the above section, the state of water/steam in the heat sink flow was calculated using the IAPWS-IF97, and the specifications of the SHS system were determined based on the properties of concrete at 200°C, Table 1 (Anderberg 1991; Pan, Zou, and Jin 2017).

Thermochemical energy storage (TCES) systems use reversible chemical reactions and offer the advantages of a high storage density and long storage times without dissipation. Generally, reversible chemical reactions in TCES occur at high temperatures between the solid and gas phases. TCES encompasses various types of chemical reactions, including hydration, carbonation, and oxidation, and each reaction working pair having distinct temperature and pressure characteristics (Kim, Takasu, and Kato 2021). The strontium bromide and water ($\text{SrBr}_2/\text{H}_2\text{O}$) working pair shows

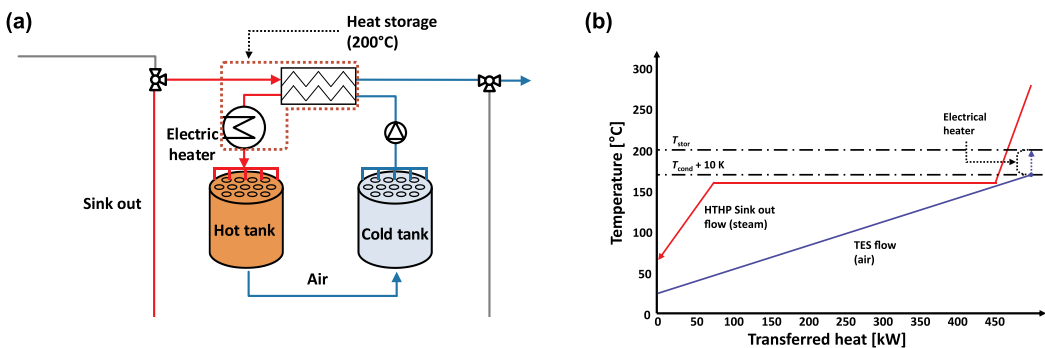


Figure 2. Heat storage operation of sensible heat storage system: (a) schematic diagram and (b) T-S diagram.

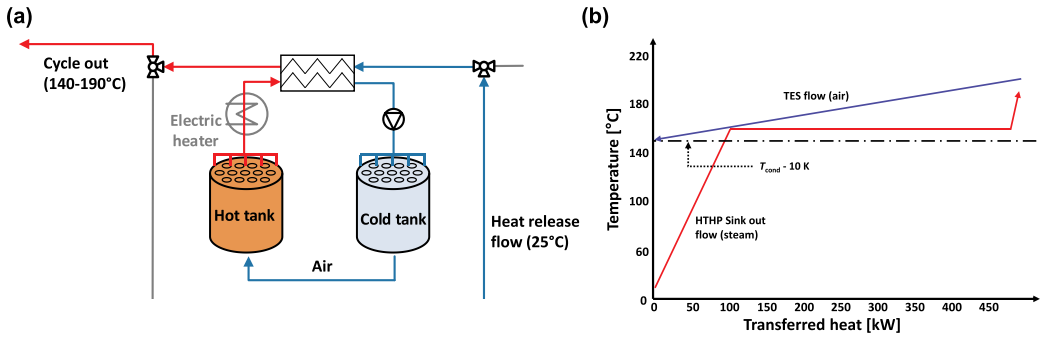


Figure 3. Heat release operation of sensible heat storage system: (a) schematic diagram and (b) T-S diagram.

Table 1. Properties of concrete for SHS systems (Kim et al. 2023a).

Temperature (°C)	Specific heat capacity, C_p , (J/(kg K))	Density, ρ , (kg/m ³)	Thermal conductivity, λ , (W/(m K))
100	832	2250	1.80
200	903	2250	1.60
300	1058	2250	1.40

high specific thermal powers at temperature above 150°C and this reaction has been in spotlight as promising material to store thermal energy in temperature range from approximately 150°C to 300°C (Richter et al. 2018; Stengler, Bürger, and Linder 2020). The monohydrated $\text{SrBr}_2 \cdot \text{H}_2\text{O}$, can store heat through dehydration, while the hydration of anhydrous SrBr_2 releases heat, as given in Equation 1.



The operational schematic diagram of the TCES system with a packed bed reactor is illustrated in Figure 4. During the heat storage operation, the dehydration of $\text{SrBr}_2 \cdot \text{H}_2\text{O}$ is induced by a heat sink at 200°C, and the resulting water vapour condenses in a water reservoir at 35°C, which is 10 K higher than the ambient temperature, T_{amb} . Unlike the SHS system, the TCES system can control the $T_{\text{cycle out}}$ by regulating the hydration temperature corresponding to the hydration pressure. Since heat for the hydration, Q_{evap} , is assumed to utilise waste heat in industrial processes, similar to the heat source for the HTHP cycle, the hydration temperature, T_{hyd} , is limited to a maximum of 110°C. In the current study, four different hydration temperatures were selected for the discharge operation, $T_{\text{hyd}} = 80, 90, 100,$ and 110°C. Additionally, the molar mass, M , and density, ρ , of anhydrous and monohydrated SrBr_2 , which are used to estimate the specification of the TCES system, are shown in Table 2 (Perry 2011). Due to the increase in volume during hydration, $\text{SrBr}_2 \cdot \text{H}_2\text{O}$ requires lower density compared to its anhydrous form.

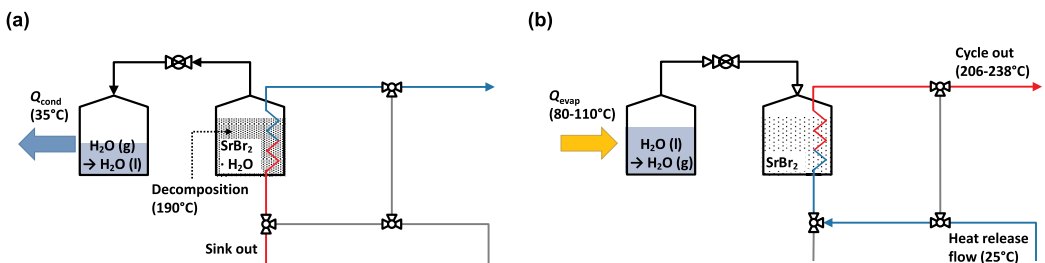


Figure 4. Image of the thermochemical energy storage system: (a) heat storage operation and (b) heat release operation.

Table 2. Chemical and physical properties of SrBr₂/H₂O TCES system.

Material	Molar mass, M , (g/mol)	Density, ρ , (kg/m ³)	Enthalpy of hydration, ΔH , (kJ/mol)
SrBr ₂	247.43	4216	71.98
SrBr ₂ ·H ₂ O	265.43	3911	

2.3. Economic models

This section presents an economic model for comparing a HTHP with TES system against hot water boilers (HWB). The HWB, assumed to operate with an efficiency of 0.98, is representative of fossil fuel-based heating equipment used in industrial processes at approximately 200°C. The economic analysis assumes an investment lifetime, n , of 20 years with a discount rate, d , of 3.5% and an inflation rate, i , of 2.8%. The net present value (NPV), used to evaluate the economic performance of the systems, is calculated using Equation 2.

$$\text{NPV} = -\text{INV} + \sum_{n=1}^{n=20} \frac{CF_n \cdot (1+i)^{n-1}}{(1+d)^n} \quad (2)$$

where i represents the inflation rate, n denotes the number of time periods, CF_n is the annual net saving electricity cost at the year n , and INV represents the initial investment for the respective systems.

Various investigations have been conducted to estimate the cost of industrial heat pumps, employing methodologies such as analyses of existing installations and devices, regression studies on large-scale district heating heat pumps, and cost projections by the European Commission, among others (Grosse et al. 2017; Lang 1947; Pieper et al. 2018; Schlosser 2021). Despite the diversity in these approaches, there is consistent common trend across all cost functions: the specific unit cost decreases with increasing heat pump capacity. This effect is associated with economies of scale. In particular, the most significant decreases are observed at capacities around 500 kW_{th} (Walden, Wellig, and Stathopoulos 2023).

To deduce the INV in Equation 3, the cost model provided by the European commission was selected for estimating the cost of the HTHP system, C_{HTHP} , while initial investment data for the TES systems are presented in Table 3. Specifically, only the storage medium cost of the TES system for 4000 kWh, 500 kW for 8 hours, is considered as C_{TES} as the cost of other TES system components can vary significantly depending on the configuration. The CF_n , derived from the difference in electricity requirements between HWB and HTHP, is calculated based on system efficiency, Equation 4. The economic parameters utilised in this study are summarised in Table 4.

$$\text{INV}_{\text{HTHP+TES}} = C_{\text{HTHP}} + C_{\text{TES}} = 0.352 \times (\dot{Q}_{\text{sink}})^{-0.122} + C_{\text{TES}} \quad (3)$$

$$CF_n = E_{\text{HWB}, n} - E_{\text{HTHP}, n} \quad (4)$$

Table 3. Cost information for of TES systems.

System	Function	Cost	Unit	Source
TES	Concrete	1.36	[€/kW _{th}]	(Strasser and Selvam 2014)
	SrBr ₂	0.52	[€/kW _{th}]	(Gilles et al. 2018)

Table 4. Economic parameters.

Parameter	Value	Unit	Source
Electricity price	0.21	[€/kWh]	(Eurostat 2022a)
Natural gas price	0.08	[€/kWh]	(Eurostat 2022b)
Discount rate	3.5	[%]	(Great Britain 2014)
Inflation rate	2.8	[%]	(Eurostat 2022c)
Lifespan of system	20	[years]	(Jovet et al. 2022)

3. Performance evaluation and analysis

3.1. High-temperature heat pump (HTHP) cycle

The performance of HTHP cycle operated with different temperature conditions, T_{evap} at 90°C and 100°C, T_{cond} at 130, 140, 150, and 160°C, was evaluated. The intermediate pressure was defined from the suction and discharge pressures, with the assumption that each compression stage has the same pressure ratio. The overall thermodynamic properties, such as the pressure, temperature, and enthalpy, of each point of the HTHP cycle were determined through thermodynamic heat and energy balance of the multistage high-temperature heat pump (Kim et al. 2023a). The important parameters, mass flow rate of the HTHP main cycle and the power consumption of two compressors, \dot{m}_{main} and W_{comp} , were estimated from Equations 5–6; the isentropic and mechanical efficiency, η_{iso} and η_{mech} , are 0.78 and 0.90, respectively. From the obtained thermal energy from the condenser and IC, $\dot{Q}_{\text{sink}} = 500$ kW, and calculated W_{comp} , COP of the HTHP cycle was defined from Equation 7. Additionally, efficiency of the system was compared to that of an ideal cycle by introducing the thermodynamic efficiency, η_{carnot} , in Equations 8–9. The Carnot efficiency, $\text{COP}_{\text{carnot}}$, represents the maximum energy efficiency of an ideal process that converts power to heat between two different temperatures, T_{L} and T_{H} (Szargut 2002).

$$\dot{m}_{\text{main}} = \frac{\dot{Q}_{\text{sink}}}{((H_{\text{IC out}} - H_{\text{IC in}}) - (H_{\text{dis}} - H_{\text{cond out}}))} \quad (5)$$

$$W_{\text{comp}} = \left(\frac{(H_{\text{IC in}} - H_{\text{suc.}}) \times \dot{m}_{\text{main}}}{\eta_{\text{mech.}}} \right) + \left(\frac{(H_{\text{dis}} - H_{\text{IC out}}) \times \dot{m}_{\text{main}}}{\eta_{\text{mech.}}} \right) \quad (6)$$

$$\text{COP} = \dot{Q}_{\text{sink}} / W_{\text{comp}} \quad (7)$$

$$\eta_{\text{carnot}} = \frac{\text{COP}}{\text{COP}_{\text{Carnot}}} \quad (8)$$

$$\text{COP}_{\text{carnot}} = \frac{T_{\text{H}}}{T_{\text{H}} - T_{\text{L}}} \quad (9)$$

According to the assumption in section 2.1, the mass flow rate of heat sink flow, \dot{m}_{sink} , has the same pressure as P_{dis} of main cycle and it was calculated from the capacity of water/steam, c_p , and enthalpy of vaporisation, ΔH_{vap} , at respective T_{cond} , Equation 10. Because the c_p is variable by temperature, averaged specific heat capacities for the liquid and gaseous state, $\bar{c}_{p\text{liquid}}$ and $\bar{c}_{p\text{gas}}$, was adopted for the precise estimation.

$$\dot{m}_{\text{sink}} = \frac{\dot{Q}_{\text{sink}}}{((T_{\text{cond}} - T_{\text{sink in}}) \times \bar{c}_{p\text{liquid}} + (T_{\text{sink out}} - T_{\text{cond}}) \times \bar{c}_{p\text{gas}} + \Delta H_{\text{vap}, T_{\text{cond}}})} \quad (10)$$

The mass flow rate changes of main and heat sink by temperature lift, T_{lift} , changes are shown in Figure 5(a). Overall \dot{m}_{main} decreases as T_{lift} increases because the enthalpy differences between inlet and outlet of intercooler and condenser, denoted as the denominator of Equation 5, increase. Specifically, the HTHP cycle with $T_{\text{evap}} = 100^\circ\text{C}$ exhibits a lower enthalpy after second compressor, H_{dis} , compared to the $T_{\text{evap}} = 90^\circ\text{C}$ cycle, resulting in a higher mass flow rate for the main cycle. On the other hand, \dot{m}_{sink} , does not show significant changes with T_{lift} or temperature conditions. This is because \dot{Q}_{sink} is fixed at 500 kW, and the specific heat capacity and ΔH_{vap} values do not vary much with temperature.

The discharge temperature of the HTHP cycle, T_{dis} , derived from pressure and enthalpy on discharge, is depicted in Figure 5(b). Since both cycles exhibit similar T_{dis} when they have the same T_{lift} , T_{dis} is analysed to be strongly depended on the T_{lift} value rather than other parameters such as T_{evap} and T_{cond} , as confirmed in a previous study (Kim et al. 2023b). The HTHP cycle with a

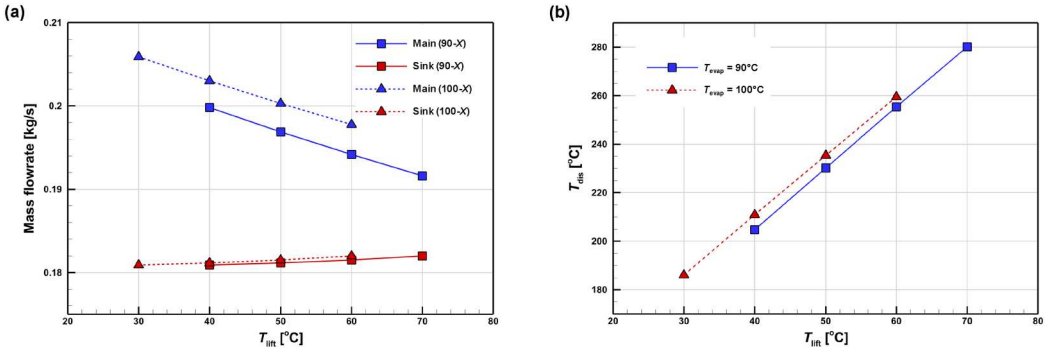


Figure 5. Performance of HTHP by T_{lift} : (a) Mass flow rate of main and heat sink, and (b) Discharge temperature, T_{dis} .

higher T_{evap} shows higher T_{dis} . It is confirmed, in particular, that a minimum T_{lift} of 40°C is required to supply heat at 200°C to the TES system directly during storage operation.

Figure 6 depicts the coefficient of performance (COP) and thermodynamic efficiency, η_{carnot} of the two-stage HTHP. The HTHP cycle with low-temperature lift, $T_{evap} = 100^\circ\text{C}$ in Figure 6, has a higher COP and η_{carnot} . The overall COP values decrease with T_{lift} exponentially, as confirmed in the previous study, Figure 6(a). Additionally, the difference between T_{evap} in the 90°C and 100°C cycles is reduced with an increase in T_{cond} , from 34% to 17% higher when T_{cond} changes from 130°C to 160°C. This is because the consumed compressor power, W_{comp} , has increased proportionally while \dot{Q}_{sink} is fixed at 500 kW, result in a proportional increase of W_{comp} to \dot{Q}_{sink} . The thermodynamic efficiency, η_{carnot} values also decrease with T_{cond} ; however, unlike COP, η_{carnot} values decrease proportionally with a certain difference, Figure 6(b). By considering that a minimum temperature lift of 40°C is required to supply heat at 200°C, the COP and thermodynamic efficiency values of the HTHP are limited to 4.4–7.5 and 0.71–0.72, respectively.

3.2. Sensible heat storage (SHS) system

In storage operation, the HTHP cycle supplies 500 kW of heat for 8 hrs ($\tau_{stor} = 28,800$ s) and both TES systems stored thermal energy without any heat loss, 14,400 MJ. The required concrete amounts for the SHS system can be calculated from Equations 11–12 based on material properties in Table 1, $m_{concrete} = 96,647$ kg and $V_{concrete} = 43.0$ m³. As aforementioned in section 2.1, the HTF in the SHS system was heated to 10 K higher condensation temperature

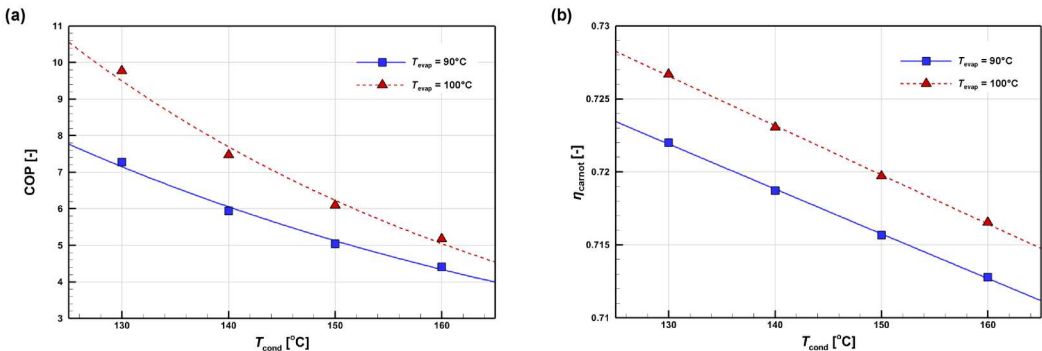


Figure 6. Performance of HTHP by condenser temperature: (a) COP, and (b) Thermodynamic efficiency, η_{carnot} .

through the heat exchanger first, then it is further heated to 200°C by using electric heater. The required air flow rate for storage operation was obtained from Equation 13, and consumed power from air pump and electric heater calculated from Equations 14–15. The values for the air pump are that the differential head, $h_{\text{air pump}}$, acceleration of gravity, g , and efficiency of the pump, $\eta_{\text{air pump}}$, are 70 m, 9.81 m/s², and 0.7, respectively. For what concerns the air mass flow rate, \dot{m}_{air} , and densities, ρ_{air} , is changed according to operation modes and temperature conditions.

$$m_{\text{concrete}} = (\dot{Q}_{\text{sink}} \times \tau_{\text{stor}}) / (c_p \text{ concrete at } 200^\circ\text{C} \times (T_{\text{stor}} - T_{\text{amb}})) \quad (11)$$

$$V_{\text{concrete}} = m_{\text{concrete}} / \rho_{\text{concrete}} \quad (12)$$

$$\dot{m}_{\text{air, stor}} = \dot{Q}_{\text{sink}} / (\bar{c}_{p \text{ air from } T_{\text{amb}} \text{ to } T_{\text{cond}+10 \text{ K}}} \times (T_{\text{cond}+10 \text{ K}} - T_{\text{amb}})) \quad (13)$$

$$W_{\text{air pump}} = \frac{(\dot{m}_{\text{air}} \times h_{\text{air pump}} \times g \times \rho_{\text{air}})}{\eta_{\text{air pump}}} \quad (14)$$

$$W_{\text{EH}} = \frac{(H_{\text{air at } 200^\circ\text{C}} - H_{\text{air at } T_{\text{cond}+10 \text{ K}}}) \times \dot{m}_{\text{air}}}{\eta_{\text{EH}}} \quad (15)$$

Table 5 presents the key parameter changes in storage operation of SHS system. A decrease in the air flow rate was observed with an increase in the condensation temperature because the outlet temperature of the heat exchanger was set at 10 K above the condensation temperature. Consequently, the power consumption of the air pump also decreases in alignment with the reduction in the air flow rate. The power consumption of electric heater exhibited a more pronounced decline, which can be attributed to the concurrent decrease in both the air flow rate and the enthalpy difference in Equation 15 with increasing condensation temperature.

In the heat release operation, the SHS system is capable of operating for up to 16 hours, as detailed in section 2.2. The system can achieve a range of cycle out temperature, $T_{\text{cond}} - 10 \text{ K} < T_{\text{cycle out}} < T_{\text{stor}} - 10 \text{ K}$, by regulating the heat output rate, $\dot{Q}_{\text{SHS, rel}}$. As described in Equation 16, the required $\dot{Q}_{\text{SHS, rel}}$ for the desired $T_{\text{cycle out}}$ can be determined from the enthalpy balance of the heat sink flow, and the corresponding mass flow rate of air, $\dot{m}_{\text{air, rel}}$, within the SHS system can also be derived. This induced air flow rate for the heat release operation results in power consumption by the air pump, as described by Equation 14.

$$\dot{m}_{\text{sink}} \times (H_{T_{\text{cycle out}}} - H_{\text{amb}}) = \dot{Q}_{\text{SHS, rel}} = \dot{m}_{\text{air, rel}} \times (T_{\text{stor}} - T_{\text{cycle out}-10 \text{ K}}) \quad (16)$$

While the SHS system maintains consistent operating values for heat storage operation at each condensation temperature, T_{cond} , both the heat output rate, $\dot{Q}_{\text{SHS, rel}}$, and the air pump power consumption, $W_{\text{air pump, rel}}$, vary with $T_{\text{cycle out}}$ and are divided into two groups based on the T_{cond} . Since the heat sink flow maintains the same pressure as the discharge pressure of the HTHP cycle, P_{dis} , it exhibits the same condensation temperature during heat release operation. The sharp increase in the enthalpy of the heat sink flow above the condensation temperature leads

Table 5. Parameter changes in storage operation of SHS system.

Condensation temperature, T_{cond} , [°C]	Air flow rate, $\dot{m}_{\text{air, stor}}$, [kg/s]	Air pump power, $W_{\text{air pump, stor}}$, [kW]	Electric heater power, W_{EH} , [kW]
130	4.06	15.52	274.35
140	3.72	14.23	209.79
150	3.44	13.13	155.01
160	3.19	12.19	108.04

to a significant increase in both $\dot{Q}_{\text{SHS, rel}}$ and $\dot{m}_{\text{air, rel}}$ when the targeted temperature exceeds the condensation temperature, **Figure 7(a)**. The variation in $\dot{m}_{\text{air, rel}}$ affects the power consumption of the air pump needed to meet the increased $\dot{Q}_{\text{SHS, rel}}$ directly. Since the stored air temperature is fixed 200°C and the temperature after the heat exchanger is set to $T_{\text{cond}}-10$ K, each cycle with different T_{cond} results in varying air pump power consumption with respect to T_{cond} , **Figure 7(b)**. It was also observed that both values slightly increase with $T_{\text{cycle out}}$ because the enthalpy of the fluids increases with $T_{\text{cycle out}}$.

3.3. Thermochemical energy storage (TCES) system

The Gibbs free energy change of a reaction, ΔG , is obtained from the reaction enthalpy change, ΔH , and the entropy change, ΔS , as shown in Equation 17.

$$\Delta G = \Delta H - T\Delta S \quad (17)$$

where ΔG has the following relationship with the reaction equilibrium constant, K_{eq} , for the gas–solid reaction assuming ideal gas properties Equation 18. The reversible reaction condition is established at around $K_{\text{eq}} = 1$ and the linear form of the Van't Hoff plot is obtained.

$$\ln K_{\text{eq}}(T, P) = \ln\left(\frac{P}{P^0}\right) = \frac{\Delta G}{RT} = -\frac{\Delta H}{RT} + \frac{\Delta S}{R} \quad (18)$$

From the reaction enthalpy, ΔH , molecular mass and density of $\text{SrBr}_2 \cdot \text{H}_2\text{O}$, $M_{\text{SrBr}_2 \cdot \text{H}_2\text{O}}$ and $\rho_{\text{SrBr}_2 \cdot \text{H}_2\text{O}}$, in **Table 2**, the necessary amounts of $\text{SrBr}_2 \cdot \text{H}_2\text{O}$ for the heat storage operation can be estimated as a mass, $m_{\text{SrBr}_2 \cdot \text{H}_2\text{O}}$, of 53,101 kg and volume, $V_{\text{SrBr}_2 \cdot \text{H}_2\text{O}}$, of 13.6 m³ from Equations 19–20, in terms of anhydrous SrBr_2 before heat release operation, 49,500 kg and 11.7 m³.

$$m_{\text{SrBr}_2 \cdot \text{H}_2\text{O}} = \left(\left(\frac{\dot{Q}_{\text{sink}}}{\Delta H} \right) / M_{\text{SrBr}_2 \cdot \text{H}_2\text{O}} \right) \times \tau_{\text{stor}} \quad (19)$$

$$V_{\text{SrBr}_2 \cdot \text{H}_2\text{O}} = m_{\text{SrBr}_2 \cdot \text{H}_2\text{O}} / \rho_{\text{SrBr}_2 \cdot \text{H}_2\text{O}} \quad (20)$$

Figure 8 shows the Van't Hoff diagram of $\text{SrBr}_2/\text{H}_2\text{O}$ solid–gas reaction, $\Delta H = 71.98$ kJ/mol and $\Delta S = 143.93$ J/(mol·K) given in the NBS table. This TCES system possible to store heat by the accomplishment of dehydration at a certain temperature, T_{dehy} , and achieve a higher output temperature than dehydration temperature, $T_{\text{hyd}} > T_{\text{dehy}}$, particularly, since T_{hyd} is controllable from hydration pressure. Therefore, the heat release operation of the TCES system is also known as

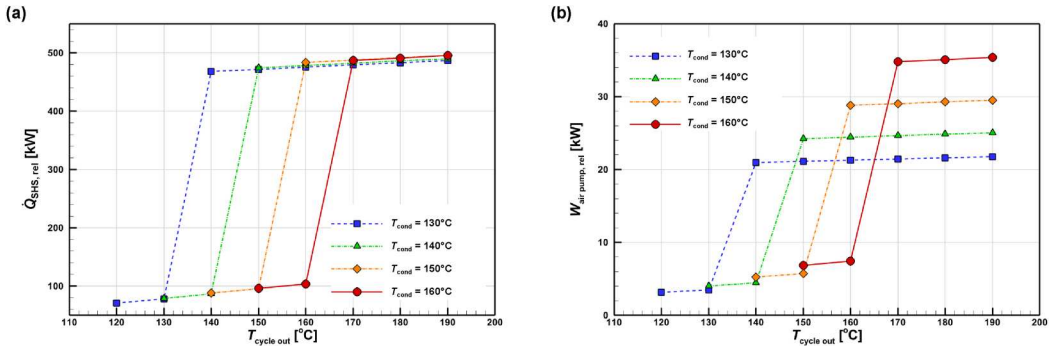


Figure 7. Heat release performance of the SHS system: (a) Heat output rate, $\dot{Q}_{\text{SHS, rel}}$, and (b) Air pump power consumption, $W_{\text{air pump}}$.

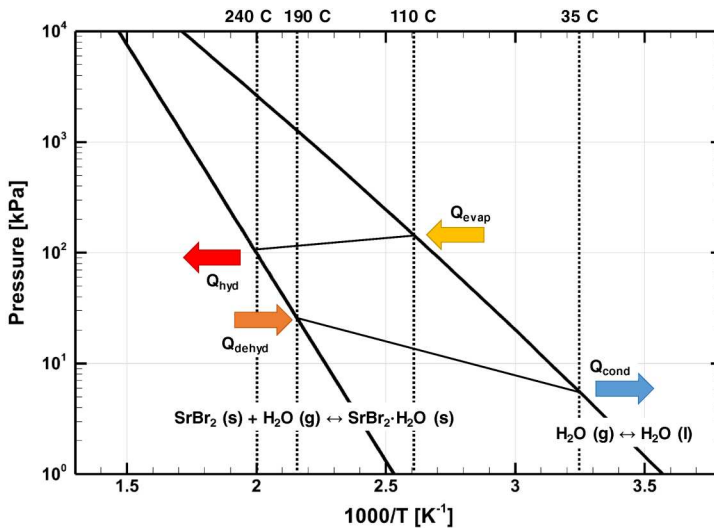


Figure 8. Van't Hoff diagram for SrBr₂/H₂O TCES system (Kim et al. 2023a)

the temperature upgrade operation of a chemical heat pump (Zamengo, Yoshida, and Morikawa 2021).

In this study, during the heat storage operation, monohydrus SrBr₂, SrBr₂·H₂O, was decomposed at 190°C, 10 K lower than T_{sink} , and the produced water vapour was condensed at 35°C, 10 K higher than T_{amb} . Because it was assumed that waste heat from the industrial process was used for evaporation, the temperature for evaporation, T_{evap} , was limited to 110°C, 10 K lower than T_{source} . Four different evaporation temperatures were selected, $T_{\text{evap}} = 80^\circ\text{C}$, 90°C , 100°C , and 110°C , and hydration temperatures were obtained as $T_{\text{hyd}} = 206^\circ\text{C}$, 217°C , 227°C , and 238°C from the corresponding saturated water vapour pressures of 47.4, 70.2, 101.4, and 143.4 kPa. The heat output rate of the TCES system, $\dot{Q}_{\text{TCES, rel}}$, is obtained from the first half of Equation 14, and Table 6 shows the cycle out temperature, $T_{\text{cycle out}}$, operable heat release time, τ_{rel} , and $\dot{Q}_{\text{TCES, rel}}$ by evaporation temperature, T_{evap} .

3.4. Comparison of both TES systems

Figure 9 compares the heat output rate and operable heat release time of both TES systems. Generally, the TCES system exhibits a higher heat output rate, \dot{Q}_{rel} , and cycle out temperature, $T_{\text{cycle out}}$ than the SHS system, as shown in Figure 9(a). Unlike the SHS system, which is limited to a heat release operation temperature of 190°C due to the stored thermal energy temperature, $T_{\text{SHS, stor}}$, of 200°C, the TCES system can release beyond 200°C. From the equilibrium pressure indicated in Equation 18, the expected $T_{\text{cycle out}}$ exceeds 196°C. Furthermore, the SHS system, with $T_{\text{cycle out}}$ lower than T_{cond} , demonstrated a very low heat output rate of approximately 70–104 kW. This is attributed to the fixed m_{sink} and the low enthalpy values of liquid state at lower

Table 6. Performance of TCES system on heat release operation (Kim et al. 2023a).

Evaporation temperature, T_{evap} [°C]	Hydration temperature, T_{hyd} [°C]	Operable time, τ_{rel} [hr]	Heat output rate of TCES, $\dot{Q}_{\text{TCES, rel}}$ [kW]
80	206	8.03	498
90	217	7.96	502
100	227	7.90	506
110	238	7.83	510

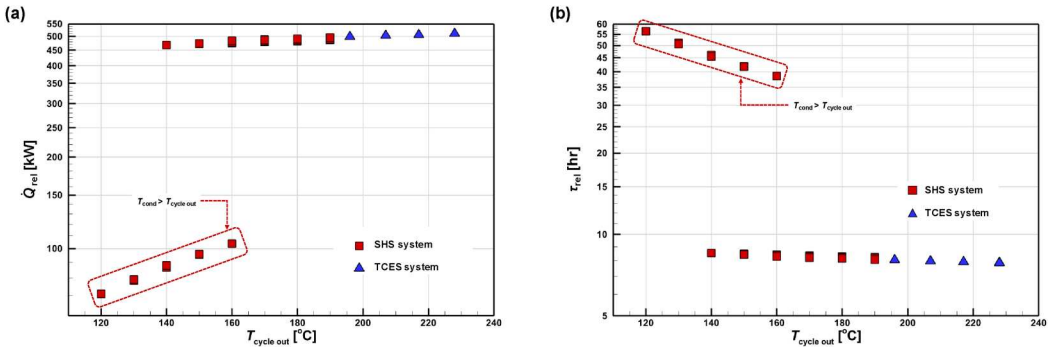


Figure 9. Comparison of thermal energy storage systems: (a) Heat output rate, \dot{Q}_{rel} , and (b) Heat release time, τ_{rel} .

temperatures. These variations in heat output rate are directly related to the available heat release time, τ_{rel} , given that both TES systems have the same stored heat of 14,400 MJ, Figure 9(b). While the SHS system with $T_{cycle\ out}$ lower than T_{cond} shows a τ_{rel} over 38 hours, more than twice the designed operating time of 16 hours, in other cases, both systems reveal a τ_{rel} of 7.8–8.5 hours.

The cycle efficiency, η_{eff} of the thermal energy storage system is expressed as the ratio of the energy provided to the TES systems to the energy released to demand, Equation 21; the power consumption of the air pump and electric heater, $W_{air\ pump}$ and W_{EH} , are considered only for the SHS system.

$$\eta_{eff} = \frac{(\dot{Q}_{rel} - W_{air\ pump, rel}) \times \tau_{rel}}{(\dot{Q}_{sink} + W_{comp} + W_{air\ pump, stor} + W_{EH}) \times \tau_{stor}} \quad (21)$$

Figure 10 depicts the changes in η_{eff} for both TES systems as a function of the cycle out temperature during heat release operations. Both TES systems exhibit a 2.0–3.1% higher η_{eff} when the cycle has a higher T_{evap} , 100°C, as the power consumption of the compressor, w_{comp} , decreases with decreasing T_{lift} . While the TCES system maintains consistent η_{eff} values between 0.82 and 0.91, the SHS system shows overall lower η_{eff} values than the TCES system due to the power consumed by electric heater during storage operations. Particularly, the SHS system with a lower $T_{cycle\ out}$ than T_{cond} exhibits significantly lower η_{eff} values, 0.16–0.27, because of the reduced heat release capacity caused by the limited

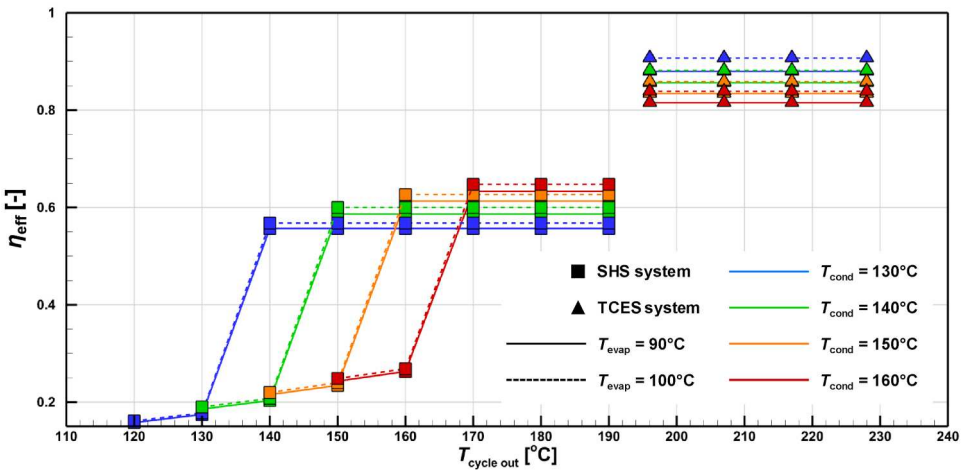


Figure 10. Comparison of cycle efficiency between concrete SHS and SrBr₂/H₂O TCES systems.

Table 7. Specifications of TES systems.

	SHS	TCES	Note
Material	Concrete	SrBr ₂ -H ₂ O (SrBr ₂)	TCES/SHS
Weight, m [kg]	96,648	53,101 (49,500)	0.55 (0.51)
Volume, V [m ³]	43.0	13.6 (11.7)	0.32 (0.27)
Cost, C_{TES} [€]	5458	2,080	0.38
Cycle efficiency, η_{eff} (-)	0.16–0.64	0.82–0.91	1.26–5.76

heat release time, $\tau_{rel} < 16$ hours, and fixed mass flow rate of the heat sink. In conclusion, the SrBr₂/H₂O TCES system demonstrates 26–63% higher η_{eff} values than the concrete SHS system when $T_{cycle\ out}$ is higher than T_{cond} . This difference increases substantially to 203–475% when $T_{cycle\ out}$ is lower than T_{cond} .

Based on the physical properties in Tables 1 and 2, the specifications, required amounts, and volumes of thermal energy storage materials are determined, Table 7. Compared to a concrete SHS system, the SrBr₂/H₂O TCES system requires 45% less mass and 68% less volume for storage operation, and 49% less mass and 73% less volume of SrBr₂ for heat release operations. Additionally, the TCES system offers benefits in terms of both economic and cycle efficiency.

4. Economic analysis

The net present value (NPV) of the integrated system, HTHP and TCES, as an alternative to the hot water boilers (HWB) that use natural gas, has been investigated over a lifespan 20 years. The positive NPV indicate that the system has cost-effectiveness, and the relationships between NPV, discount rate, d , and COP is shown in Figure 11(a). In particular, the range of COP has been limited between 4.5 and 7.5 because an HTHP system with a COP higher than 7.5 could not supply heat of 200°C to TES system, as described in section 3.1. The NPV is more sensitive to discount rate than COP; it exponentially decreases with the discount rate but gradually increase with COP. The integrated system has NPVs of €464,559 and €182,374 with COPs of 7.5 and 4.5, respectively at a discount rate of 10%, $d = 0.1$. The internal rate of return (IRR), calculated by setting the NPV = 0 in the Equation 2 and solving for the discount rate, d , is also determined, Figure 11(b). If the calculated IRR is higher than the investor's required rate of return, the investment should be undertaken. The integrated system exhibits a variation in IRR of 15.8–23.6%.

The NPV and IRR change according to the performance of HTHP and other assumptions, such as discount rate or lifespan, as shown in Figure 12. Replacing the existing HWB system with an

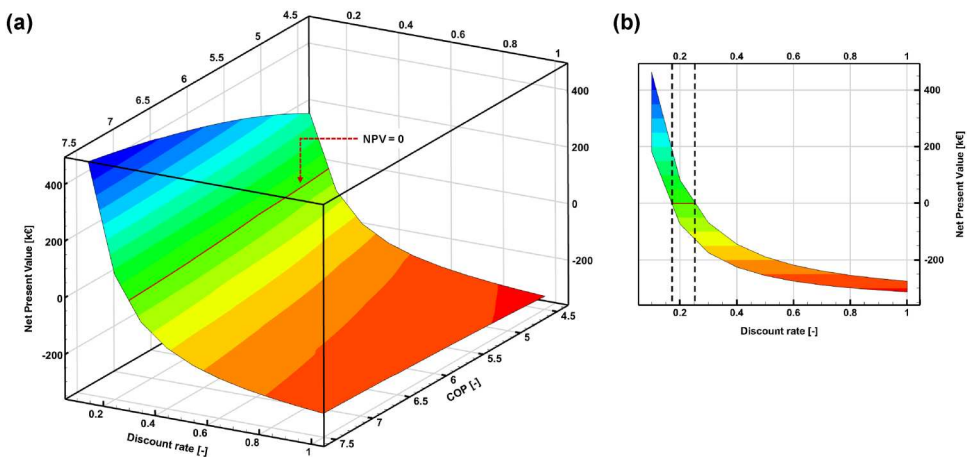


Figure 11. NPV of the integrated system, HTHP and TCES, with different discount rate and COP ($n = 20$ years, $d = 0.1$ – 1.0 , $i = 2.8\%$).

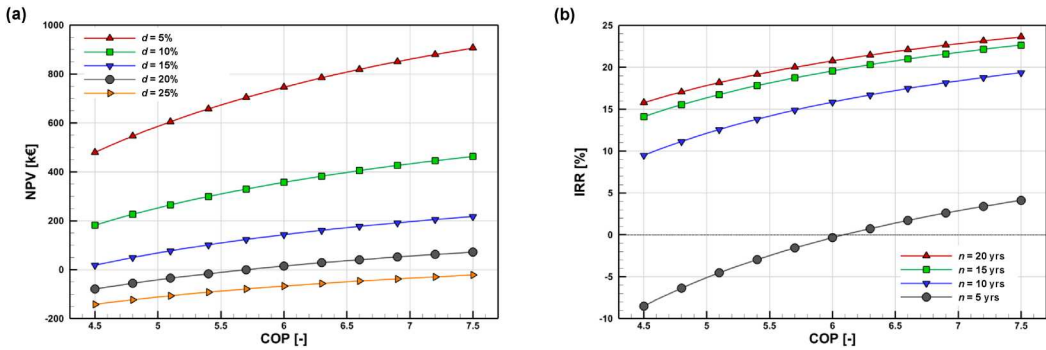


Figure 12. Changes of (a) NPVs with discount rate ($n = 20$ years) and (b) IRRs with lifespan ($d = 0.035$) according to the COPs.

HTHP and TCES integrated system and operating it for 20 years consistently shows higher economic benefits than the HWB at discount rate of 5%, 10%, and 15%, Figure 12(a). The integrated system exhibits close cutoff points for investment between discount rates of 15% and 25% when the system has COPs of 4.5 and 7.5, respectively, similar to the results shown in Figure 11(b).

Additionally, the decrease in NPV values with the discount rate has lessened because the effect of the discount rate applies to the annual net electric saving, the numerator of the right term of Equation 2, increases exponentially. From the IRR investigation, Figure 12(b), it is confirmed that the integrated system should have a lifespan of over 5 years in order to secure its value after replacing existing HWB system. Essentially, the results on Figure 12(b) has been induce on the assumption that the existing HWB will be replaced with HTHP and TCES integrated system. However, these IRR values would be increased if the analysis has conducted at the initial investment stage to choose between integrated system and HWB because the cost of HWB system, C_{HWB} , for a 500 kW_{th} is estimated to €188,627, representing 48% of C_{HTHP} (Grosse et al. 2017).

5. Conclusion

In the present work, the integrated HTHP and TES system was proposed to replace the existing fossil fuel boiler, and it was investigated in terms of thermodynamics and techno-economics. The water vapour multi-stage HTHP, with a high COP, exhibits sufficient performance to reduce CO₂ emission from industrial processes, while the two proposed TES systems showed conflict thermodynamic results. Additionally, techno-economic analyses were conducted on the integrated HTHP and TCES system to the existing natural gas boiler. The overall outcomes of this work are as follows:

1. The proposed two-stage high-temperature heat pump exhibits enough performance to supply heat over 200°C to both industrial processes and thermal energy storage systems. The overall operating values have been changed according to the operating conditions, and its COPs were estimated from 4.4 to 7.5.
2. While concrete SHS required additional power for electric heater to increase the stored temperature to 200°C and power for the air pump operation, SrBr₂/H₂O TCES system can release temperature higher than 200°C without any additional power. Particularly, the heat output rate and cycle efficiency of the concrete SHS system have been significantly decreased when the released temperature from the TES system is lower than the condensation temperature of HTHP.
3. Over 20 year of operation, the NPV of the integrated system, consisting of HTHP and TCES, is €464,559–€182,374 according to given COP. Furthermore, the integrated system consistently demonstrates higher economic benefits when the discount rate is lower than 15% and the life-span exceeds 10 years.

Future work will focus on improving the techno-economic evaluation and optimisation of the integrated HTHP and TCES system. This will involve not only levelized cost, which considers operational expenditure (OPEX) and other economic parameters, but also transient boundary conditions such as electricity costs and heat demand. The study will be helpful in demonstrating the advantages of the integrated system clearly.

Disclosure statement

No potential conflict of interest was reported by the author(s).

Data availability statement

The data that support the findings of this study are available from the corresponding author, ST Kim, upon reasonable request.

ORCID

Seon Tae Kim  <http://orcid.org/0000-0002-4388-3996>

Steffen Klöppel  <http://orcid.org/0000-0002-4930-7535>

Katamala Malleswararao  <http://orcid.org/0000-0002-3253-1522>

Marc Linder  <http://orcid.org/0000-0003-2218-5301>

References

- Anderbergo, Y. 1991. *Consequence Analysis of Eurocode 2 (Design of Concrete Structures), Part 10, Structural Fire Design (Draft April 1990)*. Lund: Fire Safety Design.
- Augustine, Chad, and Nate Blair. 2021. Energy Storage Futures Study: Storage Technology Modeling Input Data Report.
- Brueckner, S., L. Miró, L. F. Cabeza, M. Peht, and E. Laevemann. 2014. “Methods to Estimate the Industrial Waste Heat Potential of Regions – A Categorization and Literature Review.” *Renewable and Sustainable Energy Reviews* 38:164–171.
- Edenhofer, O., ed. 2014. *Climate Change 2014: Mitigation of Climate Change Working Group III Contribution to the Fifth Assessment Report of the Intergovernmental Panel on Climate Change*. New York, NY: Cambridge University Press.
- Eurostat. 2022a. *Electricity Prices for Non-Household Consumers - Bi-Annual Data (from 2007 Onwards)*. Eurostat. https://doi.org/10.2908/NRG_PC_205.
- Eurostat. 2022b. *Energy Balances 2019*. [February 28, 2022]; Available from: <https://ec.europa.eu/eurostat/web/energy/data/energy-balances>.
- Eurostat. 2022c. *HICP - Monthly Data (Annual Rate of Change)*. [February, 2024]; Available from: https://doi.org/10.2908/PRC_HICP_MANR
- Gilles, D., T. Segato, E. Courbon, M. Degrez, and P. D’Ans. 2018. “Affordable Process for the Production of Strontium Bromide Used in Low Grade Heat Recovery Applications.” *Procedia CIRP* 69:383–388.
- Great Britain. 2014. *Supporting Public Service Transformation: Cost Benefit Analysis Guidance for Local Partnerships*. London: HM Government.
- Grosse, R., B. Christopher, W. Stefan, R. Geyer, and S. Robbi. 2017. *Long Term (2050) Projections of Techno-Economic Performance of Large-Scale Heating and Cooling in the EU*. Luxembourg: Publications Office of the European Union.
- Huang, F., J. Zheng, J. M. Baleynaud, and J. Lu. 2017. “Heat Recovery Potentials and Technologies in Industrial Zones.” *Journal of the Energy Institute* 90 (6): 951–961.
- IEA. 2021. *Key World Energy Statistics 2021*, Paris.
- IEA. 2022a. *Energy Efficiency 2022*, Paris.
- IEA. 2022b. *Solar Energy Policy in Uzbekistan: A Roadmap*, Paris.
- IEA. 2023a. *CO2 Emissions in 2022*, Paris.
- IEA. 2023b. *Net Zero Roadmap: A Global Pathway to Keep the 1.5 °C Goal in Reach*, Paris.
- International Association for the Properties of Water and Steam. 2007. Revised Release on the IAPWS Industrial Formulation 1997 for the Thermodynamic Properties of Water and Steam: IAPWS R7-97(2012).

- Jovet, Y., F. Lefèvre, A. Laurent, and M. Clause. 2022. "Combined Energetic, Economic and Climate Change Assessment of Heat Pumps for Industrial Waste Heat Recovery." *Applied Energy* 313: 118854.
- Kim, S. T., R. Hegner, G. Özüylasi, P. Stathopoulos, and E. Nicke. 2023a. 14th IEA Heat Pump Conference. Chicago, IL, USA, 15–18 May 2023.
- Kim, S. T., R. Hegner, G. Özüylasi, P. Stathopoulos, and E. Nicke. 2023b. "Performance Analysis of Multistage High-Temperature Heat Pump Cycle." *Energy Science & Engineering* 11 (10): 3500–3511.
- Kim, S. T., H. Takasu, and Y. Kato. 2021. Chapter 6. *Reversible Reaction-Based Thermochemical Energy Storage Materials*. In: Ding Y, Editor. *Thermal Energy Storage*, 107–120. Cambridge: Royal Society of Chemistry.
- Kim, S. T., H. Takasu, and Y. Kato. 2023. "Solar-Thermal Energy Conversion System: Design and Practice." In *CO₂ Free Ammonia as an Energy Carrier: Japan's Insights*, edited by K. Aika, and H. Kobayashi, 119–140. Singapore: Springer Nature Singapore.
- Laing, D., C. Bahl, T. Bauer, D. Lehmann, and W.-D. Steinmann. 2011. "Thermal Energy Storage for Direct Steam Generation." *Solar Energy* 85 (4): 627–633.
- Laing, D., D. Lehmann, M. Fiß, and C. Bahl. 2009. "Test Results of Concrete Thermal Energy Storage for Parabolic Trough Power Plants." *Journal of Solar Energy Engineering* 131 (4): 041007. <https://doi.org/10.1115/1.3197844>.
- Lamb, W. F., T. Wiedmann, J. Pongratz, R. Andrew, M. Crippa, J. G. J. Olivier, et al. 2021. "A Review of Trends and Drivers of Greenhouse Gas Emissions by Sector from 1990 to 2018." *Environ. Res. Lett* 16 (7): 73005. <https://doi.org/10.1088/1748-9326/abee4e>.
- Lang, H. J. 1947. "Engineering Approach to Preliminary Cost Estimates." *Chemical Engineering* 54 (9): 130–133.
- Lee, H., K. Calvin, D. Dasgupta, G. Krinner, A. Mukherji, P. W. Thorne, et al. 2023. *Climate Change 2023: Synthesis Report. Contribution of Working Groups I, II and III to the Sixth Assessment Report of the Intergovernmental Panel on Climate Change [Core Writing Team, H. Lee and J. Romero (eds.)]*. Geneva, Switzerland: Intergovernmental Panel on Climate Change (IPCC).
- Marina, A., S. Spoelstra, H. A. Zondag, and A. K. Wemmers. 2021. "An Estimation of the European Industrial Heat Pump Market Potential." *Renewable and Sustainable Energy Reviews* 139:110545. <https://doi.org/10.1016/j.rser.2020.110545>.
- Miró, L., J. Gasia, and L. F. Cabeza. 2016. "Thermal Energy Storage (TES) for Industrial Waste Heat (IWH) Recovery: A Review." *Applied Energy* 179:284–301.
- Osterman, E., and U. Stritih. 2021. "Review on Compression Heat Pump Systems with Thermal Energy Storage for Heating and Cooling of Buildings." *Journal of Energy Storage* 39:102569. <https://doi.org/10.1016/j.est.2021.102569>.
- Pan, J., R. Zou, and F. Jin. 2017. "Experimental Study on Specific Heat of Concrete at High Temperatures and Its Influence on Thermal Energy Storage." *Energies* 10 (1): 33. <https://doi.org/10.3390/en10010033>.
- Perry, D. L. 2011. *Handbook of Inorganic Compounds*. 2nd Edition. Boca Raton: CRC Press.
- Pieper, H., T. Ommen, F. Buhler, B. L. Paaske, B. Elmegaard, and W. B. Markussen. 2018. "Allocation of Investment Costs for Large-Scale Heat Pumps Supplying District Heating." *Energy Procedia* 147:358–367.
- Rehfeldt, M., T. Fleiter, and F. Toro. 2018. "A Bottom-up Estimation of the Heating and Cooling Demand in European Industry." *Energy Efficiency* 11: 1057–1082. <https://doi.org/10.1007/s12053-017-9571-y>.
- Richter, M., E.-M. Habermann, E. Siebecke, and M. Linder. 2018. "A Systematic Screening of Salt Hydrates as Materials for a Thermochemical Heat Transformer." *Thermochimica Acta* 659:136–150.
- Schlosser, F. 2021. *Integration von Wärmepumpen zur Dekarbonisierung der Industriellen Wärmeversorgung*. Kassel: Kassel University Press. <https://doi.org/10.17170/kobra-202103023389>.
- Stengler, J., I. Bürger, and M. Linder. 2020. "Thermodynamic and Kinetic Investigations of the SrBr₂ Hydration and Dehydration Reactions for Thermochemical Energy Storage and Heat Transformation." *Applied Energy* 277:115432. <https://doi.org/10.1016/j.apenergy.2020.115432>.
- Strasser, M. N., and R. P. Selvam. 2014. "A Cost and Performance Comparison of Packed Bed and Structured Thermocline Thermal Energy Storage Systems." *Solar Energy* 108:390–402.
- Szargut, Jan. 2002. "Component Efficiencies of a Vapour-Compression Heat Pump." *Exergy, An International Journal* 2 (2): 99–104.
- Tobias, Fleitern, Jan Steinbach, Mario Ragwitz, Andreas Müller, Lukas Kranzl, Marcus Hummel, et al. 2016. Mapping and analyses of the current and future (2020-2030) heating/cooling fuel deployment (fossil/renewables) Work package 1: Final energy consumption for the year 2012 Final report: 54296.
- Tong, D., D. J. Farnham, L. Duan, Q. Zhang, N. S. Lewis, K. Caldeira, et al. 2021. "Geophysical Constraints on the Reliability of Solar and Wind Power Worldwide." *Nature Communications* 12 (1): 6146. <https://doi.org/10.1038/s41467-021-26355-z>.
- Walden, J. V., B. Wellig, and P. Stathopoulos. 2023. "Heat Pump Integration in non-Continuous Industrial Processes by Dynamic Pinch Analysis Targeting." *Applied Energy* 352:121933. <https://doi.org/10.1016/j.apenergy.2023.121933>.
- Zamengo, M., K. Yoshida, and J. Morikawa. 2021. "Numerical Evaluation of a Carnot Battery System Comprising a Chemical Heat Storage/Pump and a Brayton Cycle." *Journal of Energy Storage* 41:102955.